SHIELDED FIELD EMISSION EPMA FOR THE EXAMINATION OF NUCLEAR MATERIALS ON SECTIONS WITH POLISHED AND FRACTURED SURFACES

R. RESTANI, R. GRABHERR
Nuclear Energy and Safety Department, Paul Scherrer Institute
5232 Villigen PSI – Switzerland

ABSTRACT

A standard JEOL 8500F electron probe microanalyser (EPMA) with a Schottky field emission gun (FEG) was modified for remote control and additionally equipped with modular tungsten alloy blocks of the specimen chamber and the stage to allow high active specimens with polished surfaces to be examined electron-optically and analysed with X-ray spectrometers. The improved spatial resolution due to the higher electron beam density allows high magnification electron imaging (SEM) and quantitative X-ray elemental analysis (WDS) down to sub-micrometre structures and particles. A rotary and tilt holder makes use of the enhanced working distance and is thus applied for fractography which can also be combined with backscattered electron imaging (BSE) for phase and inclusion contrast.

1. Introduction

As an extension to the topographical and morphological imaging of a specimen by scanning electron microscopy (SEM), the electron probe microanalyser (EPMA) has additionally advanced analytical capabilities. It measures quantitatively the elemental composition in a micro area of a surface layer. An EPMA is normally equipped with a few wavelength-dispersive spectrometers (WDS) for measuring the characteristic X-rays generated by the individual elements by bombarding the sample with a focused high energy electron beam (fig. 1).
There are three different sources of electrons for SEM and EPMA which are the classic tungsten filament (W-hairpin), the LaB_6 cathode and the field-emission (FE) gun [1, 2]. The latter provides a very small probe diameter and a higher current at low accelerating voltage so that particle and trace analysis is improved and especially the lateral resolution in high magnification imaging and elemental X-ray mapping is distinctly increased [3 - 5].
Shielded EPMA instruments with W-filaments for the examination of irradiated materials have been long used and the types in operation are the Cameca SX-50R and the newer SX-100R [6]. The EPMA with a FE gun described hereafter is a standard Jeol 8500F instrument which has been subsequently customized for remote control and internally shielded to primarily protect the proportional counters of the spectrometers against γ- and stray radiation which in such a way has mitigated substantially the background level in the measurement [7].

2. Set-up of the shielded FE EPMA

The EPMA is a Jeol 8500F with Schottky field emission gun with four WDS spectrometers [7] and is installed in a lead shielded cabin adjacent to the specimen preparation cell line (Fig. 2). The specimen loading into the airlock device is carried out by cell manipulators. The shielding contains massive tungsten alloy blocks as side walls around the specimen chamber (Fig. 3). Two types of specimen stages are available, a shielded stage for high active polished specimens of 1-inch and 17 mm in diameter (fig. 4) and a rotary and tilt holder for fractography and analysis of lower active samples (fig. 5).

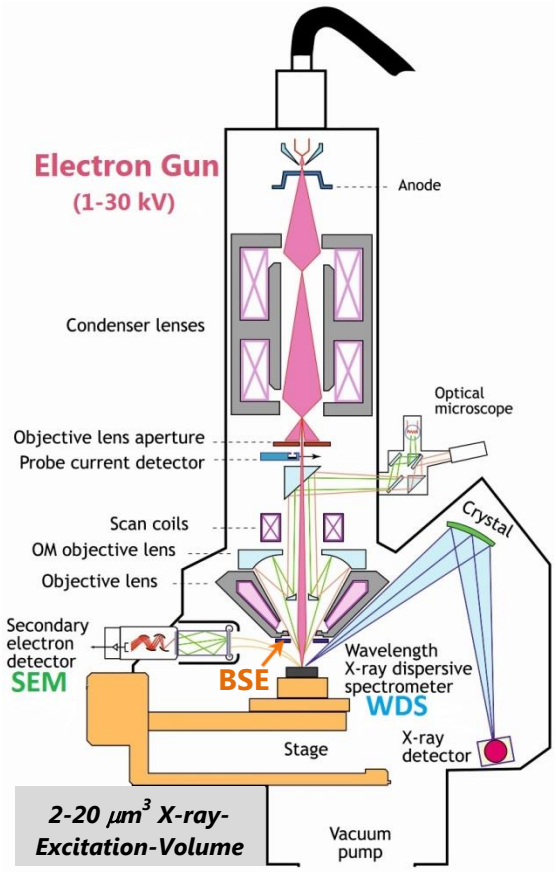

Fig. 1. Schematic sketch of EPMA

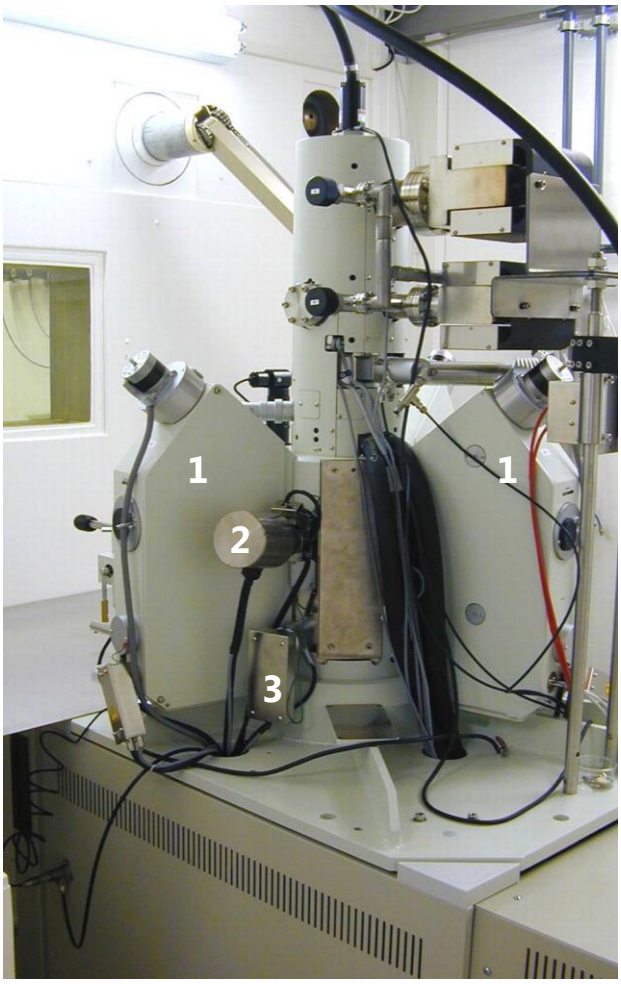

Fig. 2. Shielded FE-EPMA at PSI

1: WDS Spectrometers (2 of 4)
2: Secondary electron detector for SEM
3: Backscattered electron detector for BSE-image

Fig. 3. Shielded EPMA specimen chamber.
Machined tungsten alloy side blocks and plate (1) around pole shoe.
2: BSE detector around e-beam outlet port
3: Faraday cage for secondary electrons (SE)

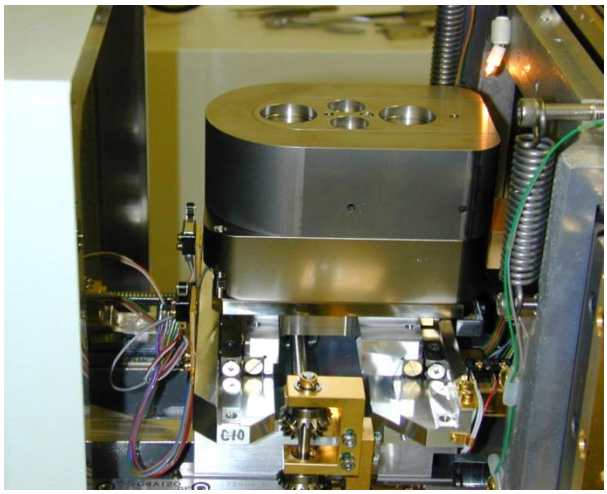

Fig. 4. Shielded stage and specimen holder for 1-inch and 17 mm specimens.

Fig. 5. Rotary- and tilt holder for fractography, 1-inch specimen.

3. Scanning Electron Microscopy (SEM) with FE-EPMA

The high resolution quality of the scanning electron microscopy unit due to the FE-gun allows examining the morphology of surfaces and their characteristics in detail in the low sub-micrometre range and is applicable for fuel as well as for reactor components. This is shown on a high burn-up fuel with subdivided grains of around 0.2 μm developed at the pore surface (fig. 6).
The depth of field may be adapted by changing the working distance and by using the rotary and tilt holder. It facilitates the inspection of fracture surfaces (fig. 7).

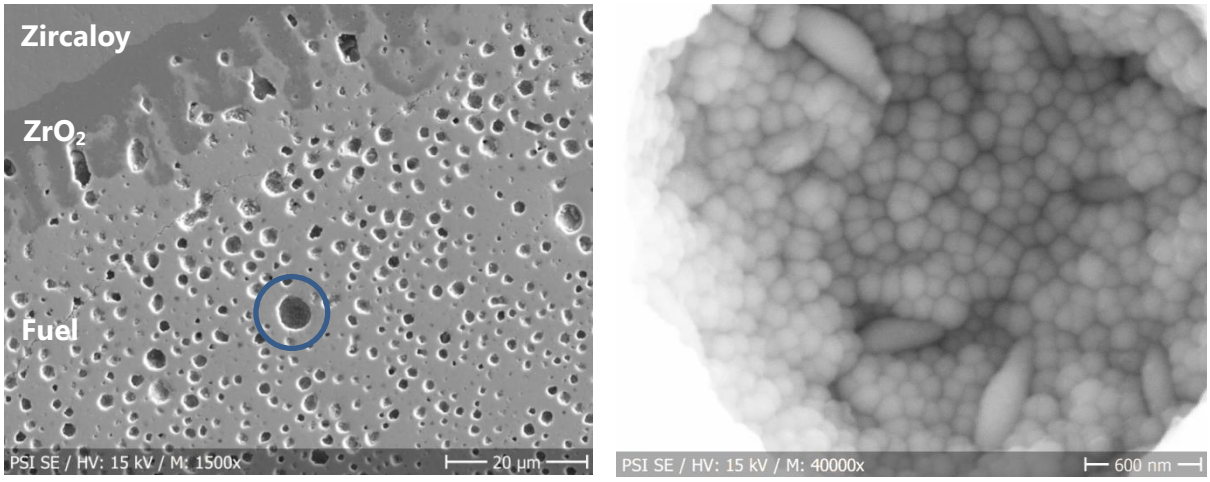

Fig. 6. SEM of a high burn-up fuel rim zone (left image) and view of the pore surface (right) with subdivided UO_2 fuel grains (final stage of polygonisation for the most part completed).

4. Backscattered Electron Imaging (BSE)

In addition to microscopic surface observation by SEM there is a durable solid-state BSE detector (fig. 1 and 3). It is not only for materials contrast imaging as is the case for zirconium hydrides in burnt fuel rods (fig. 8) and localisation of fission product precipitates in fuel but allows also under certain circumstances to observe the polycrystalline structure of polished surfaces (fig. 8 and 10). The simultaneous acquisition of SE- and BSE images gives new views of the surface adding thus the information from both detectors as to topography, material contrast and potentially the grain structure and crystallographic features like twinning (fig. 10).

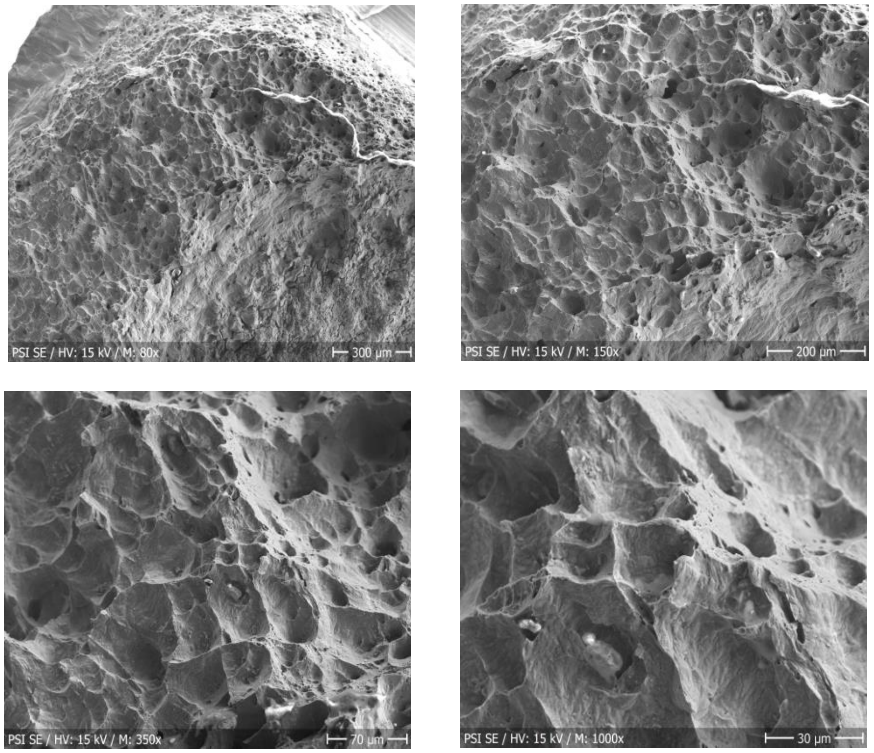

Fig. 7: SEM of a fractured steel specimen: Untreated corroded surface with residual fracture.

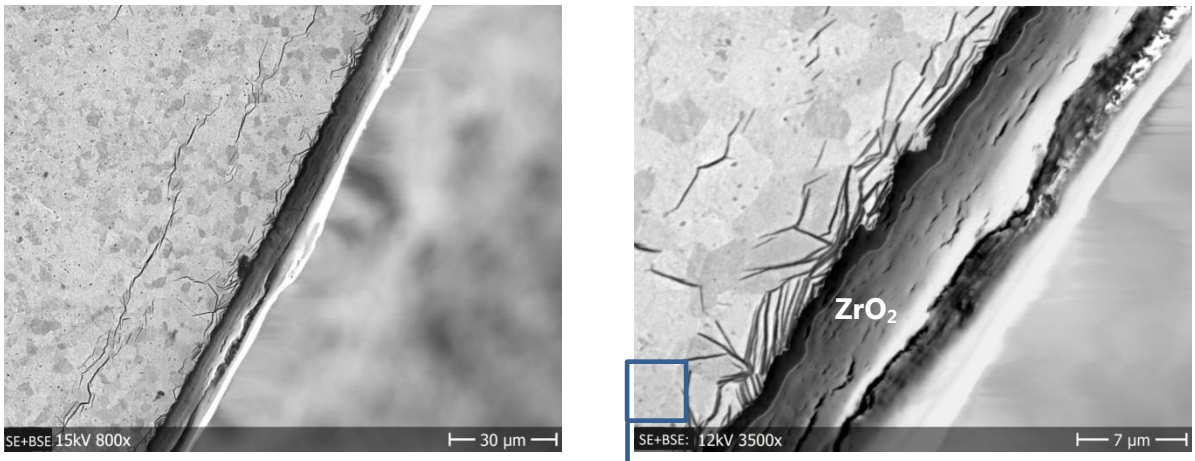

Fig. 8. Mixed SE-BSE images of outer Zircaloy-2 cladding revealing metal grain structure, hydride precipitates and oxide layer.

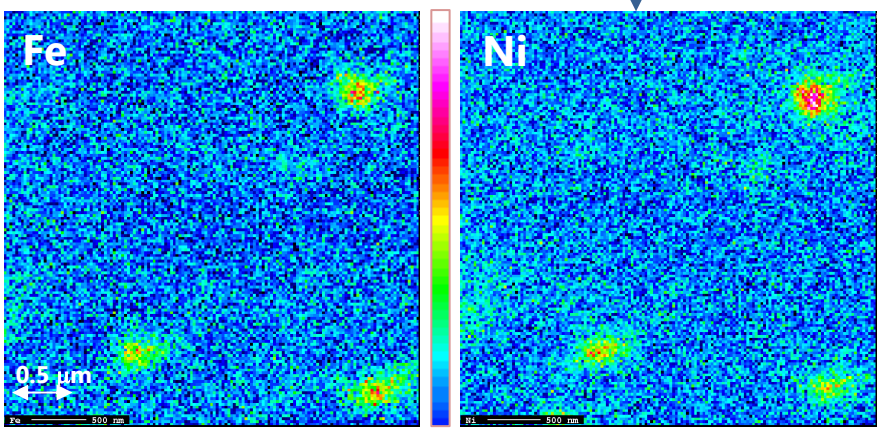

Fig. 9. X-ray mapping of secondary phase particles (SPP) in irradiated Zircaloy-2 containing Fe and Ni. Size: 50 -200 nm. (HV: 12 kV).

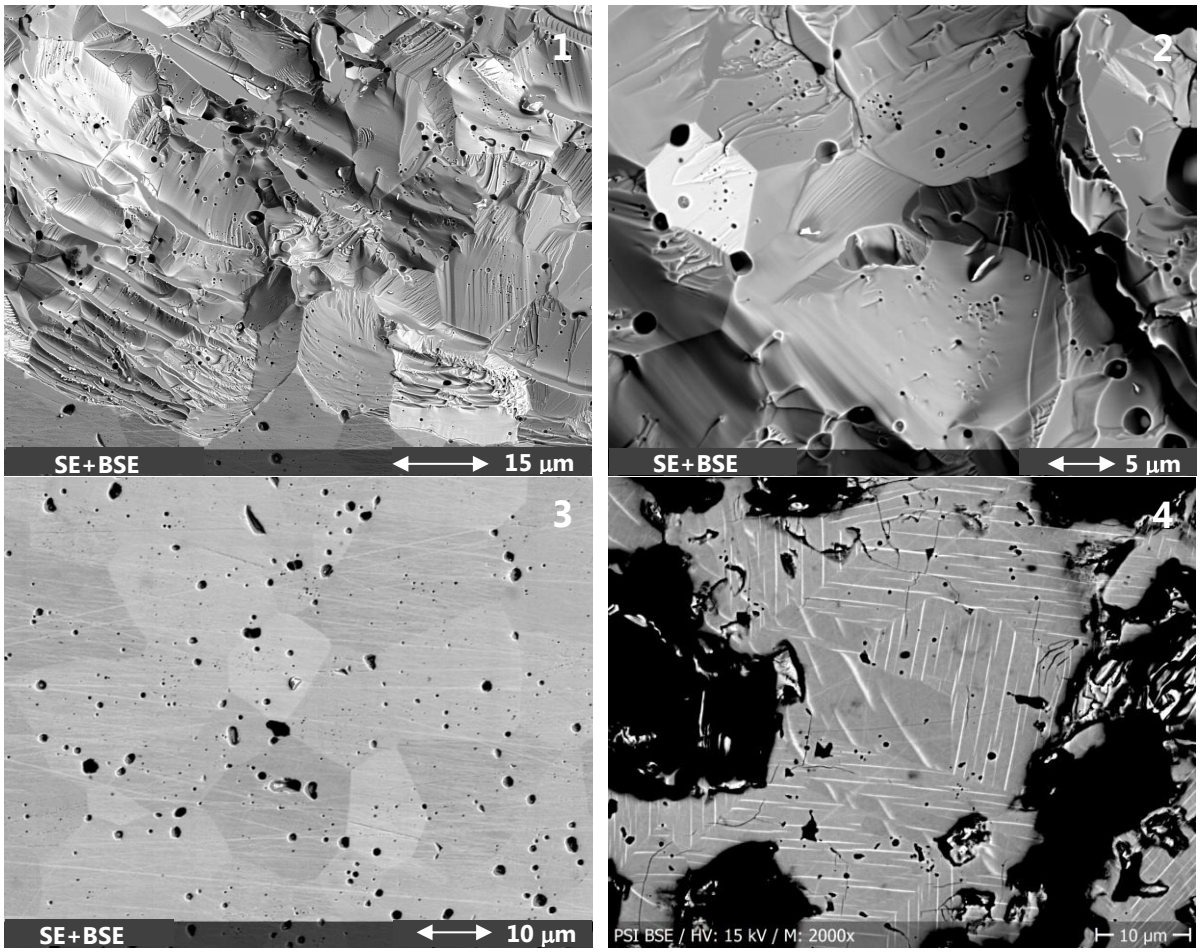

Fig. 10. Mixed SE-BSE images of UO_2 fuel grains (1-3). BSE shows grains with twinning in U-carbide (4).

5. X-ray Mapping and Microarea Analysis

The enhanced X-ray lateral resolution due to the thin high density e-beam together with a high current already at low voltage is particularly advantageous when analysing small structured features.

Secondary phase particles in Zircaloy cladding which are smaller than 0.2 μm can be readily detected at 15 kV accelerating voltage for the 3d metal elements Fe, Ni, Cr. At 12 kV the spatial resolution is slightly higher (fig. 9) because of the smaller X-ray excitation volume but the acquisition time has to be at least tripled as the signal intensity is reduced and the current cannot be increased above 100 nA lowering otherwise again the resolution as the beam diameter increases then exponentially [8, 9]. At a lower current the net intensity is more reduced for active samples because of a lower peak to background ratio which again demands a longer acquisition time.

Other useful element mappings concern the local fission product distribution in fuel which is rapidly mapped at 15 – 20 kV (fig. 11, 12).

The corrosion deposits on the cladding outer surface named CRUD which especially builds up on BWR rods are composed of ferritic spinels and pure iron oxides. The concentration of the 3d metals in solid solution can be semi-quantitatively determined and mapped with sub-micrometre resolution (fig. 13). Again the effort with long measuring times necessary at a reduced accelerating voltage of below 15 kV has to be pondered if appropriate for the analysis task with 3d metal elements for reaching a better spatial resolution although the clear advantages of low voltage cannot be denied [10]. For other elements with lower relevant X-ray absorption edges (e.g. light elements and elements with the applicable L-edge instead of K-edge) the voltage is however set to a lower level anyway.

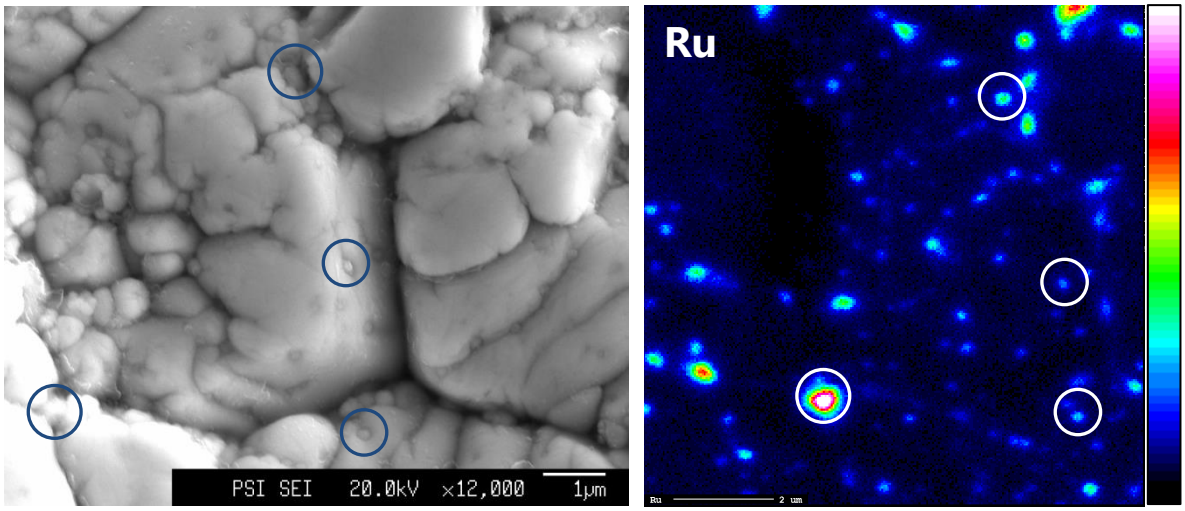

Fig. 11. SEM and corresponding Ru mapping of intermetallic fission products at grain boundaries of a fuel in the process of polygonisation.

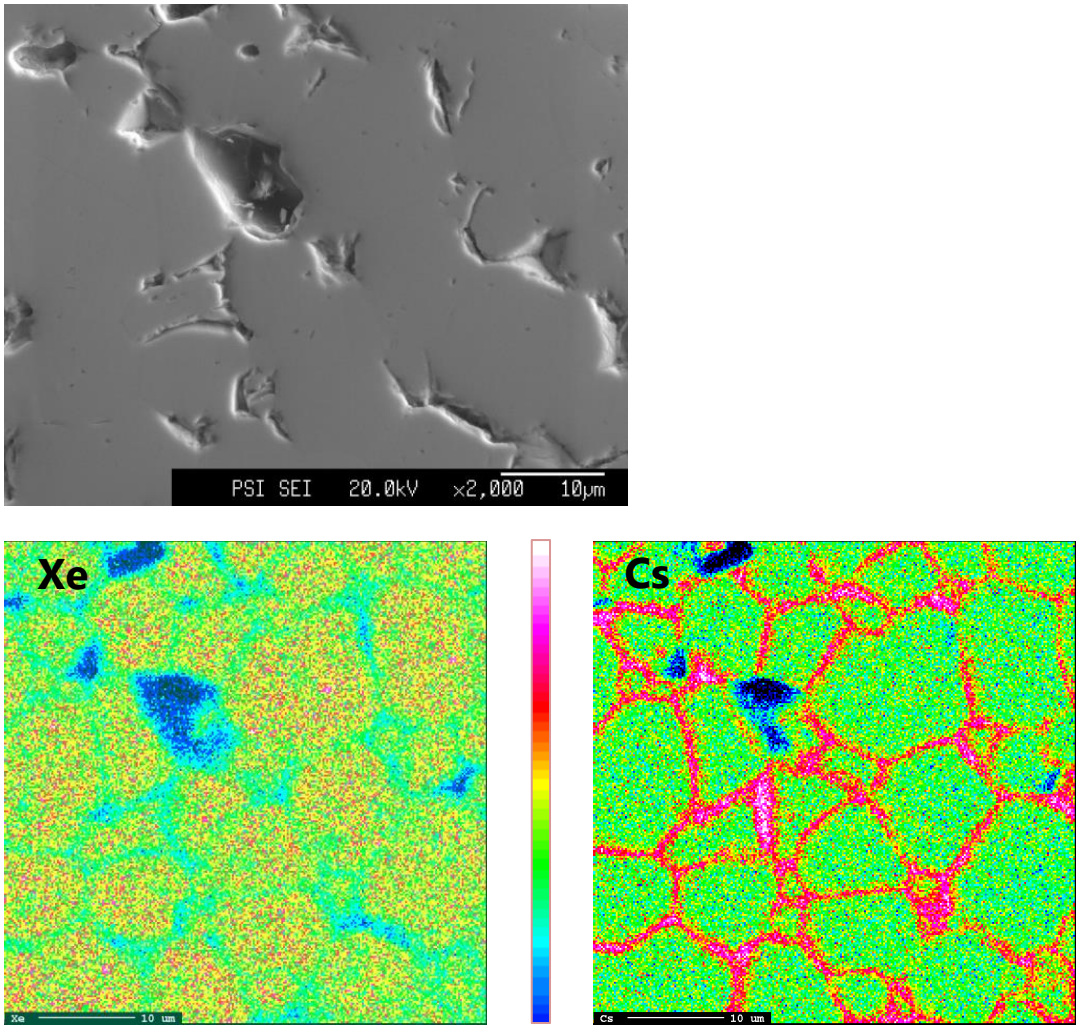

Fig. 12. SEM and qualitative elemental X-ray mappings of fission products in irradiated fuel with Xe-depletion and Cs-accumulation at grain boundaries.

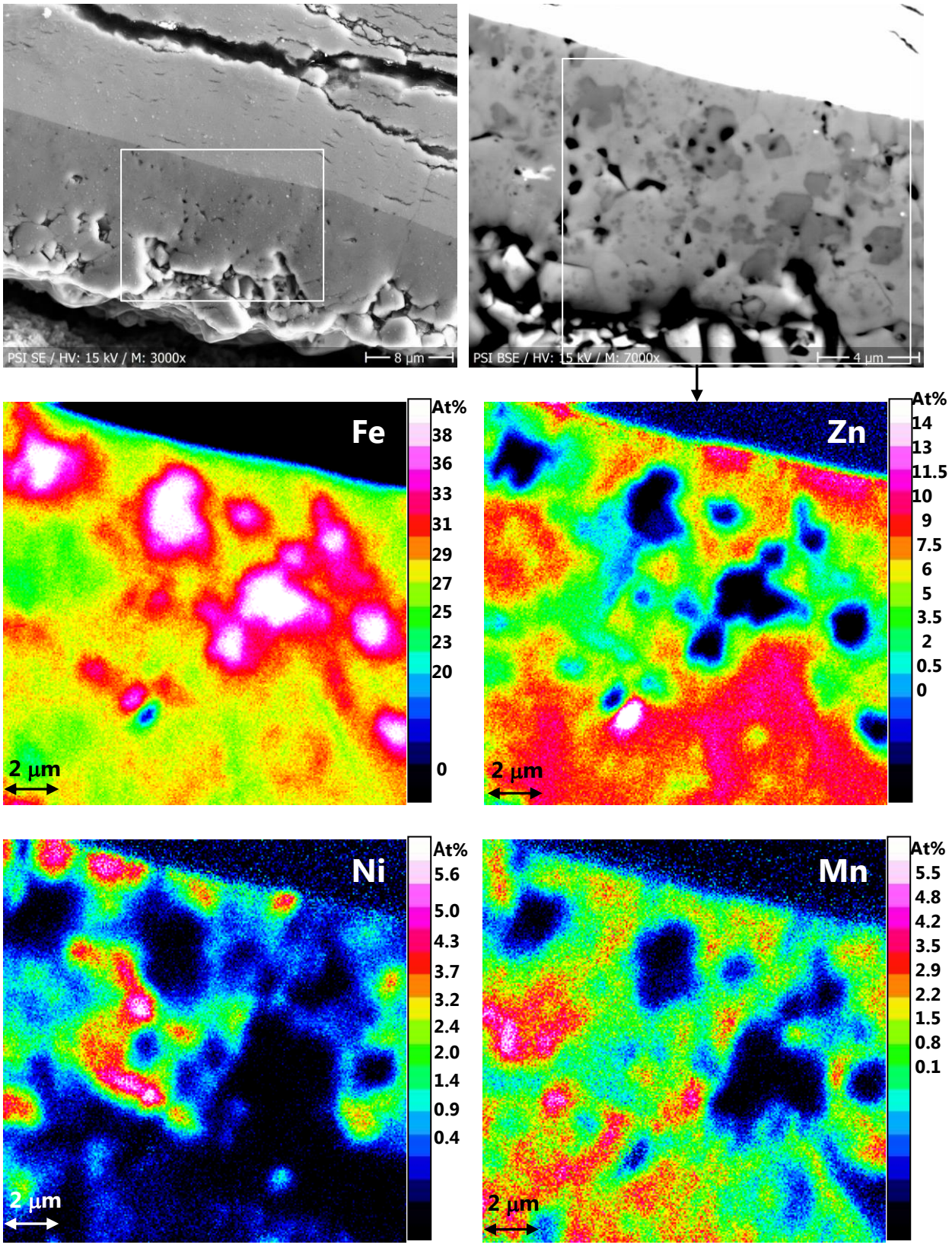

Fig. 13. Semi-quantitative X-ray element mappings of CRUD deposits on Zircaloy cladding with corresponding SE- and BSE-images. Condition: 15 kV, 200 nA, 60 ms/pix. (256 x 256 pix.), measurement of K_α emission lines.
Note: Other elements such as O and minor as Cr and Co not shown.

6. Summary and Conclusions

The advantages of the field emission EPMA with a distinctly smaller electron beam size and providing a high current at low accelerating voltage are shown on the examination of nuclear materials with a shielded instrument. The detection and analysis of sub-micron particles and fine structured phases are facilitated. The elemental qualitative and quantitative mappings show the enhancement of the spatial X-ray resolution. The excitation volume physically limits a further increase in the resolution. This can be achieved by lowering the voltage but must be checked for the benefit, as the acquisition time must be increased strongly.
The same constructional reasons are responsible for the higher electron-optical resolution of the SE- and BSE images and the available variation of the working distance discloses more possibilities for fractography.

7. Acknowledgments

We wish to thank the manufacturers of JEOL (Germany) GmbH and remX GmbH who were setting up the instrument together with our Hotlab operating group. AREVA NP and Westinghouse together with NPP Gösgen and NPP Leibstadt - and CERN are deserving our many thanks for supporting the examinations.

8. References

[1] S.J.B. Reed, Electron Microprobe Analysis and Scanning Electron Microscopy in Geology, 2nd Ed. Cambridge Univ. Press (2006).

[2] R. Rinaldi and X. Llovet, Electron Probe Microanalysis: A Review of the Past, Present and Future, Microsc. Microanal. *First View Article* (May 2015) 1-17. http://dx.doi.org/10.1017/S1431927615000409, Cambridge Univ. Press (2015).

[3] C. Hombourger and M. Outrequin, Quantitative Analysis and High-Resolution X-ray Mapping with a Field Emission Electron Microprobe. Microscopy Today, **21**(3) May 2013, 10-15.

[4] J.T. Armstrong, P. McSwiggen and C. Nielsen, A Thermal Field-Emission Electron Probe Microanalyzer for Improved Analytical Spatial Resolution, Microsc. Microanal., **27**(7) Nov. 2013, 20-24.

[5] P. McSwiggen, Characterisation of sub-micrometre Features with the FE-EPMA. IOP Conf. Series: Mat. Sci. Eng. **55** (2014) 012009. http://dx.doi.org/10.1088/1757-899X/55/1/012009.

[6] C.T. Walker, S. Brémier, P. Pöml, D. Papaioannou and P. W. D. Bottomley, Microbeam Analysis of Irradiated Nuclear Fuel. IOP Conf. Series: Mat. Sci. Eng. **32** (2012) 012028. http://iopscience.iop.org/1757-899X/32/1/012028.

[7] R. Restani and A. Waelchli, Shielded Field Emission EPMA for Microanalysis of Radioactive Materials. IOP Conf. Series: Mat. Sci. Eng. **32** (2012) 012022. http://dx.doi.org/10.1088/1757-899X/55/1/012022.

[8] T. Kimura, K. Nishida and S. Tanuma, Spatial Resolution of a Wavelength-Dispersive Electron Probe Microanalyzer Equipped with a Thermal Field Emission Gun, Microchim. Acta **155** (2006), 175-178.

[9] D. Berger and J. Nissen, Measurement and Monte Carlo Simulation of the Spatial Resolution in Element Analysis with the FEG-EPMA JEOL JXA-8530. IOP Conf. Series: Mat. Sci. Eng. **55** (2014) 012002. http://dx.doi.org/10.1088/1757-899X/55/1/012002.

[10] A. Sato, M. Takakura, N. Mori and C. Nielsen, Applications of the Field Emission Electron Probe Microanalyzer to Metals, Microsc. Microanal., **13**(Suppl 2) 2007, 168-169.